ARTICLE

Ultraviolet Photodissociation of 2-Methylallyl Radical†

Michael Lucas[b], Yuan Qin[a], Min Chen[c], Ge Sun[d], Jingsong Zhang[a*]

a. Department of Chemistry, University of California at Riverside, Riverside CA 92521, USA
b. Department of Chemistry, University of Hawaii at Manoa, Honolulu, HI 96822, USA
c. Department of Chemical Physics, School of Chemistry and Materials Science, University of Science and Technology of China, Hefei 230026, China
d. Dalian Institute of Chemical Physics, Chinese Academy of Sciences, Dalian 116023, China

(Dated: Received on September 21, 2023; Accepted on September 30, 2023)

Ultraviolet photodissociation dynamics of 2-methylallyl radical from the 3p Rydberg state were investigated in the wavelength region of 226–244 nm using the high-n Rydberg atom time-of-flight (HRTOF) technique. The 2-methylallyl radicals were generated by 193 nm photolysis of 3-chloro-2-methyl-1-propene precursors. The photofragment yield spectrum of H-atom products increases in intensity with decreasing wavelengths in 226–244 nm. The TOF spectra of H-atom products show a bimodal structure. The predominant product channel (with ~98% branching ratio) has a kinetic energy release peaking at ~7 kcal/mol, with an average ratio of E_T in the total available energy, $\langle f_T \rangle$, of ~0.18 in 226–244 nm and an isotropic product angular distribution. At the low E_T, isotropic component is from statistical unimolecular decomposition of highly vibrationally excited hot 2-methylallyl to the methylenecyclopropane+H products, following internal conversion from the excited electronic state. The minor product channel (with ~2% branching ratio) has a large kinetic energy peaking at ~50 kcal/mol, with $\langle f_T \rangle \approx 0.63$ and an anisotropic angular distribution ($\beta \approx -0.2$). At the high E_T, anisotropic component is non-statistical and is postulated to be from direct loss of H atom via the 3p Rydberg state or repulsive part of the ground state to the 1,3-butadiene+H products.

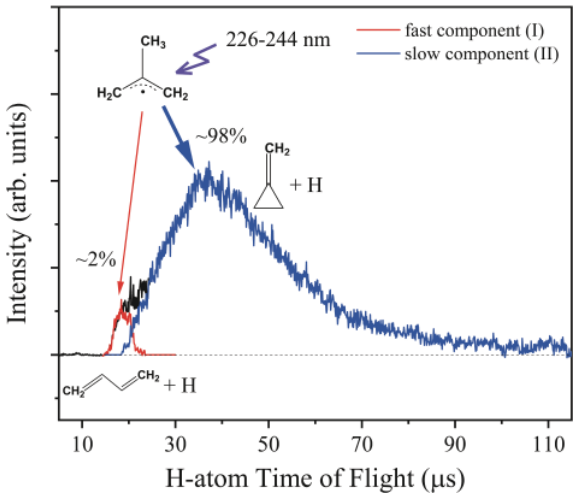

Key words: Ultraviolet, Photodissociation, Methylallyl, Radical

I. INTRODUCTION

The 1-methylallyl and 2-methylallyl radicals are methyl substituted allyl radicals and are good systems to examine the influence of methyl substitution on the photochemistry of the allyl radical. The methylallyl radicals also play roles in combustion chemistry.

The current study focuses on the 2-methylallyl radical, which has been investigated previously by various methods such as absorption [1–3], resonance-enhanced multiphoton ionization (REMPI) [4–7], photoelectron [8–10], resonance Raman [11, 12], photofragment yield [13], and infrared (IR)/ultraviolet (UV) ion dip spec-

† Part of Special Issue "In Memory of Prof. Qihe Zhu on the occasion of his 100th Anniversary".

* Author to whom correspondence should be addressed. E-mail: jingsong.zhang@ucr.edu. Fax: 1-951-827-4713. Also at the Air Pollution Research Center, University of California, Riverside, CA 92521, USA

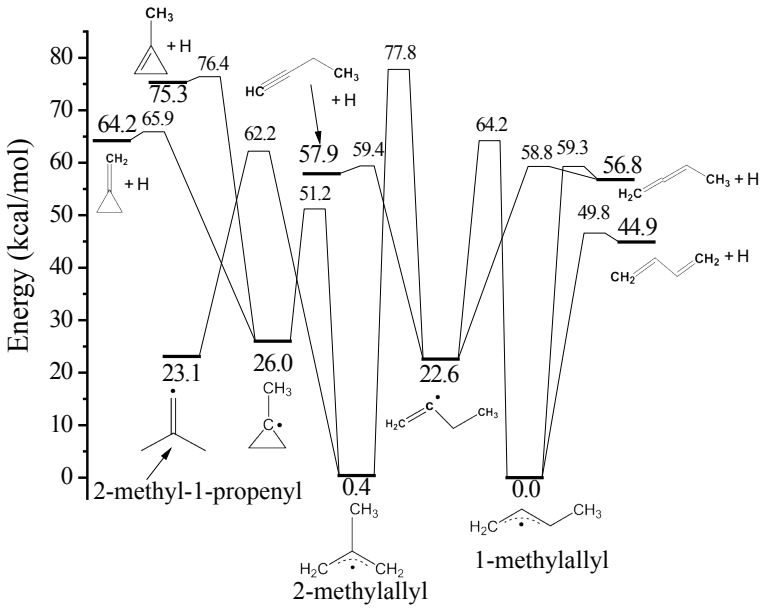

FIG. 1 Potential energy diagram of C_4H_7 dissociation pathways. The energetics and pathways are based on the theoretical calculations in Refs.[13, 15, 16].

troscopy [14]. The UV absorption spectra were first measured in 220–260 nm by Callear and Lee [1], showing a main feature peaking at 238 nm with a progression of broad bands in 220–243 nm and a weak feature with narrow and sharp bands in 254–260 nm. The strong UV absorption in 220–243 nm was confirmed by Nakashima and Yoshihara [2] and Bayrakçeken *et al.* [3]. Hudgens and Dulcey reported two-photon REMPI spectra of 2-methylallyl and identified the origin of the $\tilde{B}(^2A_1)$ 3s Rydberg state at 260 nm [4]. The assignment was confirmed in REMPI or photoelectron spectra by Chen *et al.* [5], Gasser *et al.* [6], Herterich *et al.* [7], and Röder *et al.* [10], and it is consistent with the weak feature in 254–260 nm in the absorption spectra [1]. In addition, Gasser *et al.* observed a broad absorption feature (with very short excited-state lifetime) starting at ~240 nm in the REMPI spectra and assigned it to the 2^2B_1 $3p_x$ and 1^2B_2 $3p_z$ Rydberg state [6] and was later confirmed by Röder *et al.* [10]. This feature and its assignment also agree with the previously reported main feature in 220–243 nm in the absorption spectra [1–3].

The photochemistry of 2-methylallyl was previously investigated [7, 13]. Gasser *et al.* [13] examined the photodissociation from the 2-methylallyl $\tilde{B}$ 3s state and measured the H-atom production near the band origin at 258 nm using the Doppler profiles. The H atoms had a modest kinetic energy release of 11.8 kcal/mol and appeared on the nanosecond time scale. Partially labelled 2-methylallyl ($CD_3C_3H_4$) had a statistical H/D product ratio of 4:3 following isotopic scrambling. The results, along with the time resolved experiments by Herterich *et al.* [7], suggested that 2-methylallyl undergoes internal conversion from the 3s Rydberg state and dissociates on the electronic ground state. The ground state energetics from *ab initio* calculations indicated that 2-methylallyl predominantly dissociates to H + methylenecyclopropane and may also isomerize to 1-methyallyl and dissociate to H + 1,3-butadiene [13]. In addition, 2-methylallyl can lose a methyl radical to form allene, which could compete with H-atom loss. Röder *et al.* employed femtosecond time-resolved photoelectron spectroscopy to study the photodissociation and nonradiative relaxation of 2-methylallyl at 236 nm, 238 nm, and 240.6 nm via the 3p Rydberg state [10]. The initially excited 3p Rydberg state rapidly decays to the 3s state, and the 3s state subsequently undergoes decay within a few hundred fs and ultimately deactivates to the ground electronic state on a picosecond time scale.

The energetics of unimolecular decomposition and H-atom product channels of the C_4H_7 isomers have been examined theoretically (shown in FIG. 1) [13, 15–20]. The 2-methylallyl is 0.4 kcal/mol higher in energy than 1-methylallyl (the lowest energy isomer). The 2-methylallyl does not directly lose an H atom. It can cyclize to 1-methylcyclopropyl, which then loses a methyl H atom to form H + methylenecyclopropane (with an overall

DOI: 10.1063/1674-0068/cjcp2309088

barrier of 65.5 kcal/mol, the lowest energy pathway for H-atom production from 2-methylallyl), or an H atom on the ring to produce H + 1-methylcyclopropene (with an overall barrier of 76.0 kcal/mol). In addition, 2-methylallyl can isomerize to 1-buten-2-yl via a 1,2-methyl shift over a barrier of 77.4 kcal/mol and further to 1-methylallyl. The 1-methylallyl could then lose a methyl H atom to generate H + 1,3-butadiene, or the central H atom on the allyl frame to produce H + 1,2-butadiene at higher energy. The 1-buten-2-yl could lose an H atom to produce H + 1,2-butadiene or H + 1-butyne. The energetics of the H-loss channels of the C_4H_7 system are summarized below, as shown in FIG. 1.

2-methyallyl	$\Delta H_{rxn,0}$
→ H + methylenecyclopropane	63.8 kcal/mol
→ H + methylcyclopropene	74.9 kcal/mol
→ H + 1, 3-butadiene	44.5 kcal/mol
→ H + 1, 2-butadiene	56.4 kcal/mol
→ H + 1-butyne	57.5 kcal/mol

The theoretical calculations by Gasser *et al.* [13] and Tranter *et al.* [18], also showed that 2-methylallyl can produce allene + CH_3 via C–C bond fission over a barrier of 56 kcal/mol. This channel can compete with the H + methylenecyclopropane channel, the most energetically favored H-atom product channel (with an overall barrier of 65.5 kcal/mol).

This work builds on previous studies of the photodissociation of 2-methylallyl via the 3s Rydberg state [7, 13], and investigates the photodissociation dynamics via the 3p Rydberg state at higher energy for the first time. The photodissociation of jet-cooled 2-methylallyl at UV wavelengths of 226 nm to 244 nm was investigated using the high-n Rydberg time-of-flight (HRTOF) method. Photofragment yield (PFY) spectrum of the H-atom products was obtained. The product kinetic energy and angular distributions provided detailed dynamic information for 2-methylallyl photodissociation via excitation to the 3p Rydberg state. This study also revealed a non-statistical H-atom dissociation channel of 2-methylallyl for the first time.

II. EXPERIMENTS

The experimental apparatus and the HRTOF technique have been described before [21–25] and are briefly summarized here. The 2-methylallyl radical beam was generated by photolyzing 3-chloro-2-methyl-1-propene (in ~ 2% mixture in He at ~120 kPa) using 193-nm ArF excimer laser radiation [1, 11, 12, 26]. The 2-methylallyl beam was characterized by vacuum ultraviolet (VUV) photoionization TOF mass spectrometry (TOFMS) at 121.6 nm. A UV laser radiation (226–244 nm, linewidth 0.3 cm^{-1}, 0.25–1.5 mJ/pulse, linearly polarized) was utilized to photodissociate the 2-methylallyl radicals. The H-atom photoproducts were probed by two-color resonant excitation from 1^2S to 2^2P at 121.6 nm and further to a high-n Rydberg state at 366.3 nm. A small amount of the metastable Rydberg H atoms flew toward a microchannel plate detector and were detected after field ionization. The flight length was 37.2 cm. The H-atom TOF spectra were recorded and averaged with 1×10^5–5×10^5 laser shots each. The REMPI spectrum of 2-methylallyl was measured in 239–243 nm using a (1 + 1) ionization scheme in the same HRTOF instrument. The $m/z = 55$ ion signals were measured as a function of UV laser wavelength with a Boxcar averager to produce REMPI spectrum of 2-methylallyl.

III. RESULTS

The 2-methylallyl REMPI spectrum in the region of 41100–41900 cm^{-1} (243.3–238.7 nm) is plotted in FIG. 2. The spectrum contains five peaks at 41264, 41453, 41501, 41687, and 41706 cm^{-1}, which agrees with the spectrum by Gasser *et al.* [6] and confirms the production of 2-methylallyl radicals in the molecular beam. The peaks at 41264, 41687, and 41706 cm^{-1} were previously assigned to $\tilde{B}19^1$, $\tilde{B}19^118^1$, and $\tilde{B}19^117^1$ (ν_{19}-CH_3 C–H stretch, ν_{18}-CH_3 in-plane bend, ν_{17}-CCC bend) [6]. However, these peaks may be better assigned to the $3p_x/3p_z$ Rydberg states instead [10], as they appear to be in a different series from those of the $\tilde{B}$ 3s state at lower energies and they are consistent with the progression of the main absorption feature starting at ~243 nm in the absorption spectra [1, 3] that was assigned to the 3p Rydberg states [6, 10].

The H-atom product TOF spectra from photodissociation of 2-methylallyl in the wavelength region of 226–244 nm were measured at both parallel and perpendicular polarization of the UV laser (with respect to the flight path). The main background in the HRTOF spectra was from photodissociation of the precursors and

DOI: 10.1063/1674-0068/cjcp2309088

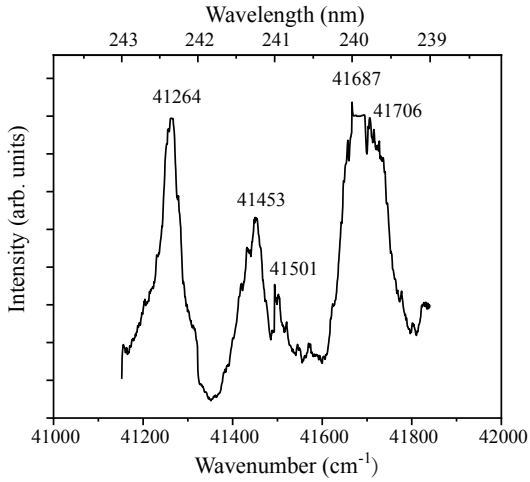

FIG. 2 1+1 REMPI spectrum of the 2-methylallyl radical generated from 3-chloro-2-methyl-1-propene in the region of 238–243 nm. The peaks at 41264 cm^{-1}, 41687 cm^{-1}, and 41706 cm^{-1} were previously assigned to $\tilde{B}19^1$, $\tilde{B}19^118^1$, and $\tilde{B}19^117^1$ (ν_{19}-CH_3 C–H stretch; ν_{18}-CH_3 in-plane bend; ν_{17}-CCC bend) [6]. But they may be better assigned to the $3p_x/3p_z$ Rydberg states [10], as they appear to be in a different series from those of the $\tilde{B}$ 3s state at lower energies and they are consistent with the progression of the main absorption feature starting at ~243 nm in the absorption spectra [1, 3].

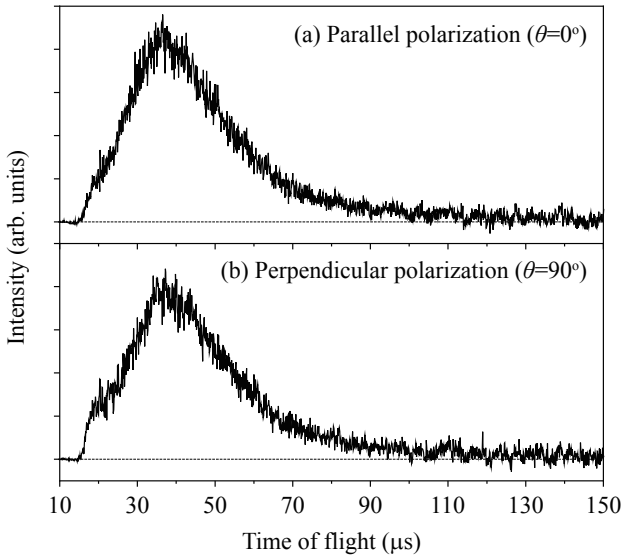

FIG. 3 H-atom TOF spectrum in the photodissociation of jet-cooled 2-methylallyl radical at 238 nm, produced from 193-nm photolysis of 3-chloro-2-methyl-1-propene. This is the net H-atom TOF with the 193-nm photolysis radiation on minus off. H-atom TOF spectra of 238 nm photodissociation of 2-methylallyl with the polarization E vector of the photodissociation radiation parallel (θ=0°) (a) and perpendicular (θ=90°) (b) to the TOF axis.

was properly removed as described previously [21, 22, 25, 27]. The H-atom TOF spectra of 2-methylallyl at 238 nm with the parallel and perpendicular polarizations are presented in FIG. 3. Both spectra have a large broad peak at ~35 μs, indicating an isotropic angular distribution. The perpendicular TOF spectrum has a small shoulder on the broad peak at ~20 μs, while the parallel spectrum shows to a lesser extent. The HRTOF spectra at other UV photodissociation wavelengths are similar to those at 238 nm.

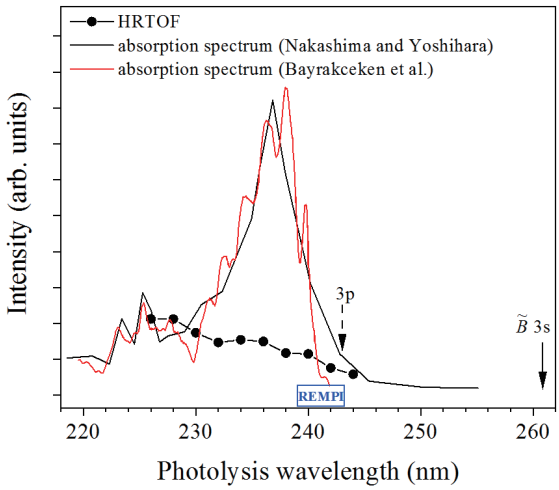

FIG. 4 H-atom product yield (PFY) spectrum as a function of photolysis excitation energy in the region of 226–244 nm. The solid circles (●) represents the integrated HRTOF signals using the 3-chloro-2-methyl-1-propene precursor. The solid lines represent the absorption spectra taken from Nakashima and Yoshihara [2] and Bayrakçeken *et al.* (with background removed) [3], which are similar to that by Callear and Lee [1]. The onsets of the 3s and 3p excited states are indicated by the arrows [6, 10]. The wavelength range of the REMPI spectrum in FIG. 2 is indicated.

The H-atom PFY spectrum of 2-methylallyl in 226–244 nm is presented in FIG. 4. The spectrum was derived from integrating the H-atom TOF spectra versus the photolysis wavelength. The spectrum was scaled to the signal at 238 nm as a reference to normalize variation in experimental conditions. The PFY intensity decreases with increasing wavelength. FIG. 4 also compares the UV absorption spectra of 2-methylallyl from Nakashima and Yoshihara [2] and Bayrakçeken *et al.* (with background removed) [3], which are similar to that by Callear and Lee [1]. Although our experiment indicates that the H-atom TOF signals and PFY spectrum are from 2-methylallyl, the PFY spectrum appears different from the UV spectra, suggesting additional dissociation products (such as CH_3) in addition to H atoms.

The H-atom product TOF spectra of the 2-methylallyl photodissociation are converted to product center-of-mass (CM) kinetic energy distribution, $P(E_T)$. The

DOI: 10.1063/1674-0068/cjcp2309088

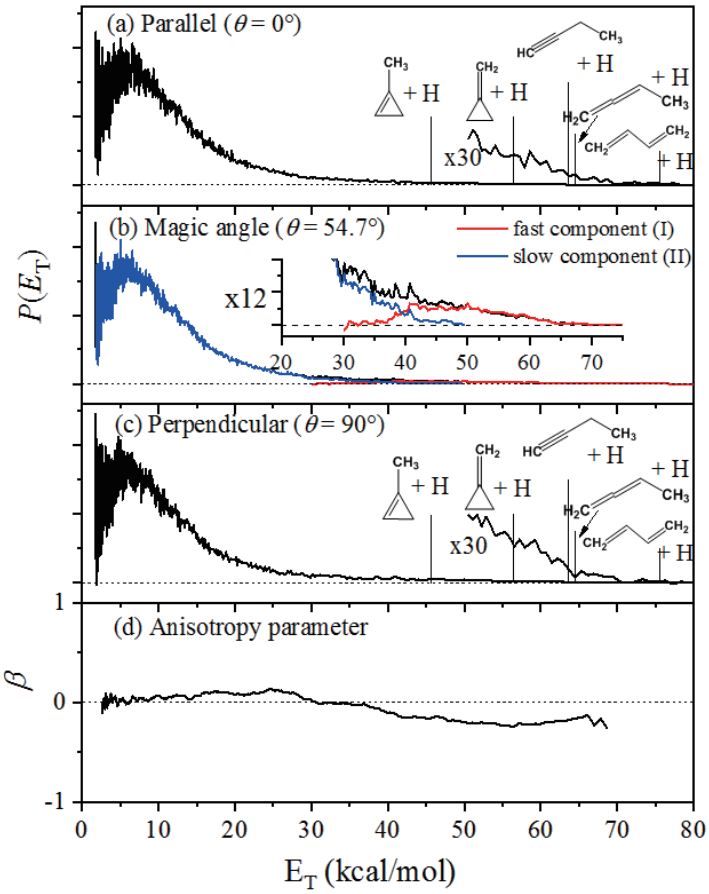

FIG. 5 Center-of-mass product kinetic energy distribution, $P(E_T)$, of 2-methylallyl radical derived from the TOF spectra in FIG. 3, with the 238 nm photolysis radiation polarization (a) parallel to the TOF axis, (b) at magic angle, and (c) perpendicular to the TOF axis. (d) Anisotropy parameter is derived from (a) and (c). $P(E_T)$ are plotted at the same scale. In (b), the magic-angle $P_m(E_T)$ distributions are de-convoluted with a fast component, $P_I(E_T)$ (red line) and a slow component, $P_{II}(E_T)$ (blue line). The vertical lines in (a) and (c) indicate the maximum kinetic energies of the H-atom product channels. See the text for details.

product CM kinetic energy E_T is derived from the H-atom flight time, t_H, with the following equation,

$$E_T = \left(1 + \frac{m_H}{m_{C_4H_7}}\right) E_H = \frac{1}{2} m_H \left(1 + \frac{m_H}{m_{C_4H_7}}\right) \left(\frac{L}{t_H}\right)^2$$

where E_H is the laboratory kinetic energy of the H-atom product and L is the TOF path length. The $P(E_T)$ and photofragment angular distribution can be expressed as $P(E_T, \theta) = \frac{1}{4\pi} P(E_T)[1 + \beta P_2(\cos\theta)]$, where $P(E_T)$ is the angle-integrated product kinetic energy distribution, β is the anisotropy parameter $(-1 \le \beta \le 2)$, θ is the angle between the recoiling direction of the H-atom product (the TOF axis) and the photodissociation laser radiation polarization, and $P_2(\cos\theta)$ is the second Legendre polynomial [28]. $P(E_T, \theta)$ at parallel $(\theta = 0°)$ and perpendicular $(\theta = 90°)$ polarization, $P_{\parallel}(E_T)$ and $P_{\perp}(E_T)$, are transformed from the TOF spectra in FIG. 5 (a) and (c). The anisotropy parameter $\beta(E_T)$ is evaluated using $\beta(E_T) = \frac{2[P_{\parallel}(E_T) - P_{\perp}(E_T)]}{P_{\parallel}(E_T) + 2P_{\perp}(E_T)}$ and is shown in FIG. 5(d). The CM kinetic energy distribution at the magic angle $(\theta = 54.7°)$, $P_m(E_T) = (1/4\pi)P(E_T)$, is calculated by combining $P_{\parallel}(E_T)$ and $P_{\perp}(E_T)$ and is plotted in FIG. 5(b). $P_m(E_T)$ is proportional to $P(E_T)$ and independent of β, thus it is employed in calculating product kinetic energy release and branching ratios.

The $P(E_T)$ at 238 nm shows a modest kinetic energy release (FIG. 5). The major channel peaks at a low E_T of ~7 kcal/mol, while the minor channel peaks at a high E_T of ~50 kcal/mol and reaches the maximum available energy (~75 kcal/mol) for the H+1,3-butadiene products. The anisotropy parameter β is ~0 at $E_T < 35$

DOI: 10.1063/1674-0068/cjcp2309088

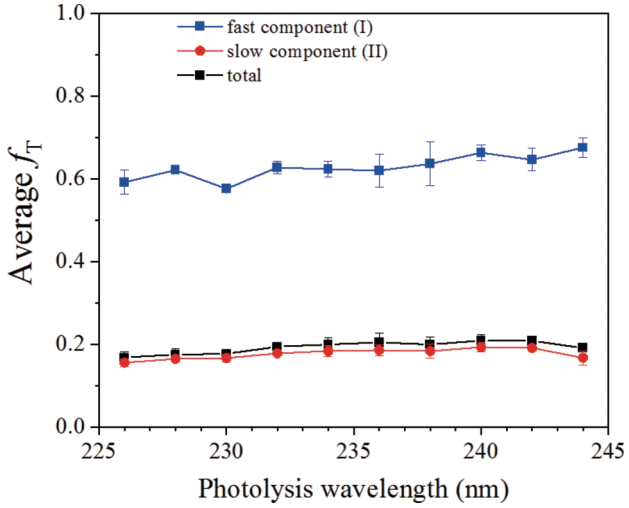

FIG. 6 Photolysis wavelength and fraction of average kinetic energy release in the total available energy, $\langle f_T \rangle$, as well as $\langle f_T \rangle$ of the deconvoluted fast and slow components, in the UV photodissociation of the 2-methylallyl radical. The average kinetic energies are calculated from the experimental $P(E_T)$ distributions. The total available energy at each photolysis wavelength is derived from the corresponding photon energy and the dissociation energy of 2-methylallyl to methylenecyclopropane+H for the slow component (II) as well as for the overall $\langle f_T \rangle$ calculations. The fast component (I) is assumed to be mainly the 1,3-butadiene+H channel when calculating $\langle f_T \rangle$. The error bars represent the statistical uncertainty (1σ) from multiple measurements.

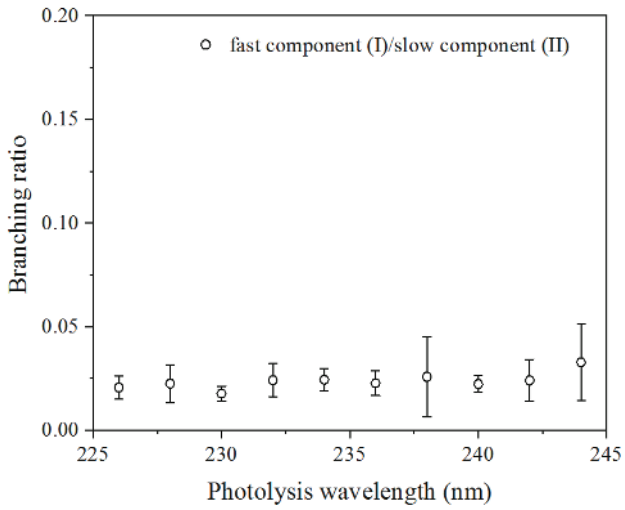

FIG. 7 Photolysis wavelength and branching ratio of the fast and slow components in the UV photodissociation of the 2-methylallyl radical. The intensities of the fast and slow components are obtained from integrating the deconvoluted fast and slow components in the fitted $P(E_T)$ distributions (for example, in FIG. 5 for 238 nm). The error bars represent the statistical uncertainty (1σ) from multiple measurements.

kcal/mol, indicating an isotropic angular distribution. At $E_T > 50$ kcal/mol for the minor component, β decreases to ~−0.2, implying an anisotropic angular distribution. The different β values suggest that there are at least two dissociation pathways. The experimental $P(E_T)$ is a combination of these dissociation pathways, and the variation in $\beta(E_T)$ with energy is a result of these channels, each characterized by distinct β parameters and energy-dependent branching ratios [23]. Consequently, $P(E_T)$ and $\beta(E_T)$ can be expressed to be $P(E_T) = P_I(E_T) + P_{II}(E_T)$ and $\beta(E_T) = x_I(E_T)\beta_I + x_{II}(E_T)\beta_{II}$, where $P_i(E_T)$ and β_i are associated with the respective ith channel, and $x_i = P_i(E_T)/P(E_T)$ is the energy-dependent branching fraction of the ith channel [23]. If the β value of the slow component is taken as a constant at ~0 and β of the fast component at –0.2, the relative contributions, $P_i(E_T)$, of both channels can be deconvoluted, as illustrated in FIG. 5(b). Using the deconvoluted components, the average product kinetic energy, $\langle E_T \rangle$, and the fraction of $\langle E_T \rangle$ in the total excess energy, $\langle f_T \rangle$, are evaluated for each component. At 238 nm, the fast channel (I) has $\langle E_T \rangle = 48.1$ kcal/mol and $\langle f_T \rangle = 0.64$ (assume the H+1,3-butadiene products; discussed later); the slow channel (II) has $\langle E_T \rangle = 10.3$ kcal/mol and $\langle f_T \rangle = 0.18$ (assume the H+methylenecyclopropane products; discussed later). As the contribution from the fast component (I) is very small in the $P(E_T)$s, the H+methylenecyclopropane product channel in the slow component (II) can be viewed as the dominant pathway when estimating the overall $\langle f_T \rangle$ of the H-loss product channel, which gives an overall $\langle f_T \rangle$ ~0.20 at 238 nm. FIG. 6 shows the $\langle f_T \rangle$ values of the H-loss product channels in 226–244 nm. The overall $\langle f_T \rangle$ is modest, in the range of 0.17–0.21 from 226–244 nm (with an average of 0.19). The $\langle f_T \rangle$ of the fast component (I) increases slightly from 0.58 to 0.68 in wavelengths from 226 nm to 244 nm, with an average of 0.63. The $\langle f_T \rangle$ of the slow component (II) changes slightly from 0.16 to 0.19 in 226–244 nm, with an average of 0.18. At 238 nm, the fast/slow branching ratio is estimated from the integrated $P_I(E_T)$ and $P_{II}(E_T)$ to be ~0.03. The fast/slow branching ratios at other wavelengths in 226–244 nm are also derived and summarized in FIG. 7. The branching ratios are from 0.02 to 0.03, with an average of 0.02. These values stay nearly a constant as the intensity of the fast component (I) is very small and has uncertainties.

The appearance time of the H-atom production in 2-methylallyl was investigated using the photodissocia-

DOI: 10.1063/1674-0068/cjcp2309088

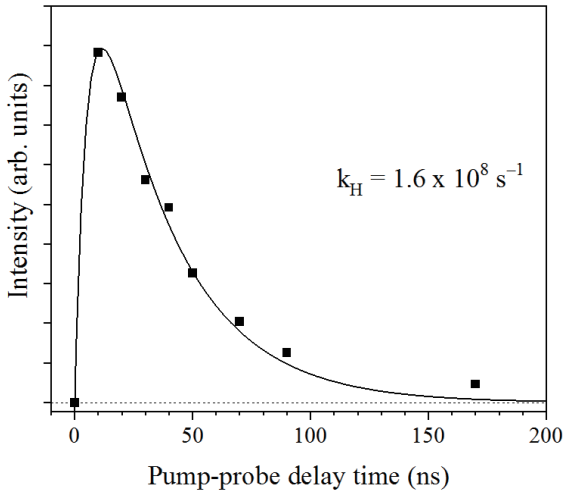

FIG. 8 H-atom product signal as a function of photolysis and probe delay time at 232 nm. The signals are obtained by integrating the HRTOF spectra at various photolysis-probe delay times. The solid line is the fitting result of the H-atom product time profile for obtaining dissociation rate constant k_H. See text for more details.

tion pump and probe experiment. The HRTOF spectra were measured at various photodissociation-probe laser delays at 232 nm, and their integrated intensities versus the delay time gave the appearance time profile of the H-atom products (FIG. 8). The rise of the temporal profile indicates the H-atom production from 2-methylallyl, while the decay is due to the H-atom departing the detection zone. The microcanonical rate constant of unimolecular H-loss dissociation of 2-methylallyl, k_H, can be extracted from the H-atom appearance temporal profile, $S_H(t)$, by fitting with the following expression [29],

$$S_H(t) = N\left[1-\exp(-k_H t)\right]\cdot\left[\frac{1}{\exp[(t-a)/b]+1}\right] \quad (1)$$

where a and b are parameters for describing the flying out decay of the H-atom signal. The dissociation rate constant $k_H \approx 1.6\times10^8$ s^{-1} at 232 nm was derived (FIG. 8). This k_H is a lower limit of the actual dissociate rate constant, since the 7-ns pump and probe laser pulses set the time resolution of the H-atom product appearance time measurements.

IV. DISCUSSION

The H + C_4H_6 product channel in the UV photodissociation of 2-methylallyl via the 3p Rydberg state was examined in 226–244 nm. The PFY spectrum of H-atom is broad and increases in intensity with decreasing wavelengths. This trend is different from (or a part of) the reported UV absorption spectra in 226–243 nm that peaks at 238 nm [1–3]. This could be due to non-H-atom photoproducts that were not detected by our experimental setup, such as the CH_3 loss product channel that could compete with the H-loss product channels [13, 18].

The $P(E_T)$ distributions of photodissociation of 2-methylallyl are similar in 226–244 nm (with those at 238 nm shown in FIG. 5). The $P(E_T)$s at both polarizations have a broad feature peaking at $E_T \approx 7$ kcal/mol and extend to ~75.6 kcal/mol (the maximum available energy at 238 nm for the H + 1,3-butadiene product channel). The $\beta(E_T)$ parameter shows two different regions (FIG. 5(d)), indicating two H-atom photodissociation features. The β value is ~0 in the E_T range of 0 to ~35 kcal/mol, whereas β decreases from $E_T \approx$ 35 kcal/mol and reaches a constant of about −0.2 at $E_T >$ ~50 kcal/mol. The $P(E_T)$ therefore is deconvoluted into two components, a minor high E_T (fast) component (I) and a dominant low E_T (slow) component (II), indicating two dissociation channels in 2-methylallyl via the 3p Rydberg state (FIG. 5).

The predominant broad feature in $P(E_T)$, component (II), peaking at low kinetic energy, shows a statistical-type kinetic energy release in the H-loss dissociation channel. This main, slow pathway has an isotropic angular distribution, which implies a dissociation timescale longer than one rotational period of the radical parent (~10 ps). The photodissociation mechanism of component (II) is consistent with a statistical mechanism. The low E_T release, broad shape of $P(E_T)$, and isotropic angular distribution suggest a unimolecular dissociation mechanism of vibrationally excited hot radical on the electronic ground state to produce the statistically favored H-loss products, after internal conversion from the excited 3p Rydberg state. Indeed, the femtosecond time-resolved study on the 3p Rydberg state of 2-methylallyl shows that the initially excited 3p state rapidly decays to the 3s state, which then subsequently deactivates to the electronic ground state on a picosecond time scale [7, 10]. The lower limit of the rate constant for the H-atom production from 2-methylallyl at 232 nm, measured to be $>1.6\times10^8$ s^{-1} in this study, is consistent with the statistical unimolecular decomposition. The unimolecular dissociation mechanism of 2-methylallyl via 3p is also similar to that of 3s in the previous studies [7, 13].

To identify the H-loss products in the slow component (II), it is noted that direct H-loss from 2-methylal-

DOI: 10.1063/1674-0068/cjcp2309088

lyl is not feasible (except at very high energy), and isomerization of 2-methylallyl is needed. On the ground-state potential energy surface (FIG. 1), the lowest energy pathway for 2-methylallyl isomerization is cyclization to 1-methylcyclopropyl radical over a transition state barrier of 50.8 kcal/mol (starting from 2-methylallyl). Two H-atom product channels are then possible from 1-methylcyclopropyl. The 1-methylcyclopropyl could lose a methyl H-atom to form H + methylenecyclopropane (at lower energy $\Delta H = 63.8$ kcal/mol), over a barrier of 65.5 kcal/mol (this is the lowest overall barrier for H-atom loss on the ground state). The 1-methylcyclopropyl can also lose an H atom from the ring to generate H + methylcyclopropene at higher energy, with a much higher barrier of 76.0 kcal/mol. Another isomerization pathway of 2-methylallyl is via a 1,2-methyl shift to 1-buten-2-yl over a barrier of 77.4 kcal/mol and further to 1-methylallyl. The 1-methylallyl could then lose a methyl H atom to produce H + 1,3-butadiene (at $\Delta H = 44.5$ kcal/mol, the thermodynamically lowest energy H-loss channel in the C_4H_7 system), or the central H atom on the allyl frame to generate H + 1,2-butadiene at higher energy. The 1-buten-2-yl could lose an H atom to generate H + 1,2-butadiene or H + 1-butyne at higher energies. The overall barrier for the H-loss pathways via 1-methylallyl and 1-buten-2-yl is the large 77.4 kcal/mol isomerization barrier from 2-methylallyl, 11.9 kcal/mol higher than the overall barrier for production of H + methylenecyclopropane. These energetics indicate that the dominant statistical dissociation channel on the C_4H_7 ground electronic state is most likely the production of H + methylenecyclopropane. Other H-loss channels, although accessible by the photoexcitation energies in this study (117.2–126.5 kcal/mol), are expected to be much less important than the H + methylenecyclopropane pathway. This is supported by the deconvoluted $P(E_T)$ of the slow component (II), which does not extend beyond the energy limit of the H + methylenecyclopropane product channel (FIG. 5(b)). This conclusion also agrees with the early study of the photodissociation of 2-methylallyl via 3s, which indicated H + methylenecyclopropane as the main unimolecular H-loss decomposition channel on the C_4H_7 ground electronic state, following nonradiative decay from the 3s Rydberg state [7, 13]. Using the energy limit of the H + methylenecyclopropane product channel, $\langle f_T \rangle$ of the dominant, low E_T component (II) is calculated and shown to be modest with values of ~0.16–0.19 at the photodissociation wavelengths of 226–244 nm (FIG. 6). The $\langle f_T \rangle$ values are comparable to that in the 3s photodissociation of 2-methyallyl at 258 nm [13]. The $\langle f_T \rangle$ values are also similar to those of 0.18–0.22 in the statistical dissociation of the allyl radical in the UV photodissociation in 216–249 nm [21].

The high E_T component (I) in the $P(E_T)$s at 238 nm has a repulsive and large energy release (peaking at ~ 50 kcal/mol). The kinetic energy release of component (I) goes beyond the maximum available energy allowed for the H + methylenecyclopropane channel (the main products of component (II)) and extends to ~ 75 kcal/mol, the onset of the H + 1,3-butadiene product channel (FIG. 5(a)–(c)). The anisotropic feature of FIG. 5(d) with the negative β parameter ($\beta < 0$ at $E_T >$ ~ 40 kcal/mol) indicates a rapid dissociation in a timescale shorter than the rotational period of 2-methylallyl (~10 ps). All these dynamic information indicates a repulsive, non-statistical photodissociation mechanism for the fast component (I), possibly directly via the 3p Rydberg state or from the repulsive part of the ground electronic state. This non-statistical photodissociation channel of 2-methyallyl has not been reported previously. The $P(E_T)$s in FIG. 5 show that the fast component possibly leads to the production of H + 1,3-butadiene. However, direct H-loss via C–H bond fission on methyl site of 2-methylallyl is not feasible due to the high energy requirement (C–H bond dissociation energy ~ 105 kcal/mol), and further it does not produce the fast H atom products nor the H + 1,3-butadiene products (FIG. 1). Although 2-methylallyl can undergo a direct C–C bond fission to produce CH_3 + allene over a barrier of 56 kcal/mol [13], which competes with the C–H bond fission channels (mainly H + methylenecyclopropane), our experiments can only monitor the H-atom product but not the CH_3 product. It is not clear how in the fast channel 2-methylallyl loses H atom directly and repulsively via the 3p Rydberg state or from the repulsive part of the ground electronic state. It is speculated that upon excitation to the 3p Rydberg state there is a minor isomerization process to 1-methylallyl on the excited surfaces that positions the system for a fast, direct and repulsive H loss to produce 1,3-butadiene + H. A conical intersection might mediate this direct dissociation process, as in the case of photodissociation of the Rydberg states of alkyl radicals [23, 30–32]. It is also noted that the negative β parameter of the fast component (I) implies that the direction of the H-atom ejection is approximately perpendicular to the transition dipole moment $\boldsymbol{\mu}$ between the ground electronic $\tilde{X}(^2A_2/^2A'')$ and the excited (3p Rydberg) states. If the excited state is the $3p_x$ ($2^2B_1/3^2A''$) Ryd-

DOI: 10.1063/1674-0068/cjcp2309088

berg state (preferred to $3p_z$ ($1^2B_2/3^2A'$) due to its larger oscillator strength) [6, 10], $\boldsymbol{\mu}$ is then of A′ symmetry and in the molecular plane. This would give rise to a negative β parameter when the H atom on the terminal CH_3 group of 1-methylallyl departs out of the molecular plane (leaving the CH_2 group in the plane of the 1,3-butadiene product). This speculative mechanism would be consistent with the observed negative β value of the fast component (I).

V. CONCLUSION

The H-atom product channels in the UV photodissociation of the jet-cooled 2-methylallyl radicals via the 3p Rydberg state were investigated at the wavelengths of 226–246 nm. The $P(E_T)$ and angular distributions were bimodal. The low E_T isotropic ($\beta \approx 0$) component (II) is consistent with internal conversion from the 3p Rydberg excited state followed by unimolecular dissociation of the hot 2-methylallyl radical to H + methylenecyclopropane. The high E_T anisotropic ($\beta \approx -0.2$) component (I) is presumably from direct loss of H atom from the 3p Rydberg state or via a repulsive part of the ground state. The statistical unimolecular dissociation channel of 2-methylallyl is similar to those previously reported in the photodissociation of the similar radicals [7, 13, 21, 33]. The non-statistical photodissociation dynamics of 2-methylallyl (component (I)) is reported for the first time.

VI. ACKNOWLEDGEMENTS

This work was supported by the US National Science Foundation (No.CHE-2155232). Yuan Qin acknowledges support from a UC Riverside Dissertation-Year Fellowship. Min Chen acknowledges support from a China Scholarships Council Fellowship.

[1] A. Callear and H. Lee, Trans. Faraday Soc. **64**, 308 (1968).
[2] N. Nakashima and K. Yoshihara, Laser Chem. **7**, 177 (1987).
[3] F. Bayrakçeken, Z. Telatar, F. Arı, and A. B. Bayrak, Spectrochim. Acta A **67**, 1276 (2007).
[4] J. W. Hudgens and C. Dulcey, J. Phy. Chem. A **89**, 1505 (1985).
[5] C. C. Chen, H. C. Wu, C. M. Tseng, Y. H. Yang, and Y. T. Chen, J. Chem. Phys. **119**, 241 (2003).
[6] M. Gasser, J. A. Frey, J. M. Hostettler, and A. Bach, J. Mole. Spectrosc. **263**, 93 (2010).
[7] J. Herterich, T. Gerbich, and I. Fischer, ChemPhysChem **14**, 3906 (2013).
[8] J. C. Schultz, F. A. Houle, and J. L. Beauchamp, J. Am. Chem. Soc. **106**, 7336 (1984).
[9] M. Lang, F. Holzmeier, P. Hemberger, and I. Fischer, J. Phys. Chem. A **119**, 3995 (2015).
[10] A. Röder, K. Issler, L. Poisson, A. Humeniuk, M. Wohlgemuth, M. Comte, F. Lepetit, I. Fischer, R. Mitric, and J. Petersen, J. Chem. Phys. **147**, 013902 (2017).
[11] D. H. Tarrant, J. D. Getty, X. Liu, and P. B. Kelly, J. Phys. Chem. **100**, 7772 (1996).
[12] J. D. Getty, X. Liu, and P. B. Kelly, J. Chem. Phys. **104**, 3176 (1996).
[13] M. Gasser, A. Bach, and P. Chen, Phys. Chem. Chem. Phys. **10**, 1133 (2008).
[14] T. Preitschopf, F. Hirsch, A. K. Lemmens, A. M. Rijs, and I. Fischer, Phys. Chem. Chem. Phys. **24**, 7682 (2022).
[15] J. L. Miller, J. Phys. Chem. A **108**, 2268 (2004).
[16] Y. Li, H. L. Liu, Z. J. Zhou, X. R. Huang, and C. C. Sun, J. Phys. Chem. A **114**, 9496 (2010).
[17] J. M. Ribeiro and A. M. Mebel, J. Phys. Chem. A **120**, 1800 (2016).
[18] R. S. Tranter, A. W. Jasper, J. B. Randazzo, J. P. Lockhart, and J. P. Porterfield, Proc. Combust Inst. **36**, 211 (2017).
[19] C. Huang, B. Yang, and F. Zhang, Combust. Flame **181**, 100 (2017).
[20] J. Cho, A. W. Jasper, Y. Georgievskii, S. J. Klippenstein, and R. Sivaramakrishnan, Combust. Flame 112502 (2022).
[21] Y. Song, M. Lucas, M. Alcaraz, J. Zhang, and C. Brazier, J. Phys. Chem. A **119**, 12318 (2015).
[22] Y. Song, M. Lucas, M. Alcaraz, J. Zhang, and C. Brazier, J. Chem. Phys. **136**, 044308-1 (2012).
[23] G. Amaral, K. Xu, and J. Zhang, J. Chem. Phys. **114**, 5164 (2001).
[24] K. Xu, G. Amaral, and J. Zhang, J. Chem. Phys. **111**, 6271 (1999).
[25] Y. Song, X. Zheng, M. Lucas, and J. Zhang, Phys. Chem. Chem. Phys. **13**, 8296 (2011).
[26] L. R. McCunn, M. J. Krisch, Y. Liu, L. J. Butler, and J. Shu, J. Phys. Chem. A **109**, 6430 (2005).
[27] M. Lucas, J. Minor, J. Zhang, and C. Brazier, J. Phys. Chem. A **117**, 12138 (2013).
[28] R. N. Zare, Mol. Photochem. **4**, 1 (1972).
[29] H. J. Deyerl, I. Fischer, and P. Chen, J. Chem. Phys. **110**, 1450 (1999).
[30] Y. Song, X. Zheng, W. Zhou, M. Lucas, and J. Zhang, J. Chem. Phys. **142**, 224306 (2015).
[31] G. Sun, X. Zheng, Y. Song, M. Lucas, and J. Zhang, J. Chem. Phys. **152**, 244303 (2020).
[32] G. Sun, Y. Song, and J. Zhang, Chin. J. Chem. Phys. **31**, 439 (2018).
[33] M. Gasser, J. A. Frey, J. M. Hostettler, and A. Bach, Chem. Commun. **47**, 301 (2011).

DOI: 10.1063/1674-0068/cjcp2309088